Engineering Geology 305 (2022) 106725

Contents lists available at ScienceDirect

Engineering Geology

journal homepage: www.elsevier.com/locate/enggeo

A new double-porosity macroscopic model of bentonite free swelling

Vicente Navarro *, Virginia Cabrera, Gema De la Morena, Laura Asensio, Ángel Yustres, Joel Torres-Serra

Geoenvironmental Group, Universidad de Castilla-La Mancha, Avda. Camilo José Cela 2, 13071 Ciudad Real, Spain

ARTICLE INFO

Keywords:
Double porosity
Macroscopic model
Free swelling
Macrostructural swelling water

ABSTRACT

A macroscopic model based on a double-porosity approach is proposed to simulate the swelling caused by the subdivision of particles and aggregates that occurs when bentonites are hydrated under a high water content and low confinement. In the model, it is assumed that although the water that occupies this new porous structure can be considered mobile (associated with the macrostructure), its contribution to variations in the energy of the system is similar to that caused by the immobile water that occupies the microstructure. Assuming isothermal conditions, a functional relationship between the increase in the void ratio and the decrease in internal energy was defined from the Clausius-Duhem equation. From this functional relationship, a macroscopic constitutive model was derived to determine the macrostructural swelling as a function of the decrease in the microstructural effective stress. The model was applied to simulate both tests with a large void ratio (up to 50) and processes with a notable variation in salinity (from deionized water to 1 M solution), and satisfactory results were obtained in all cases. This study proposes a simple strategy to incorporate the model into the equations generally used to solve hydro-chemical-mechanical boundary problems at the engineering scale and is thus of direct practical interest.

1. Introduction

The use of compacted bentonite as a barrier element is an option considered by various administrative bodies for the deep geological storage of high-intensity radioactive waste (Bennett and Gens, 2008). The efficiency of these barriers is largely determined by the swelling capacity of the bentonite. Thus, for example, swelling under low confinement conditions will be key for the sealing of potential preferential flow pathways associated with natural or technological gaps (Sellin and Leupin, 2013). Therefore, it is of interest to have a macroscopic model of swelling that can be implemented in numerical models simulating the long-term evolution of the repositories.

Microstructural testing techniques (see, for example, Delage and Tessier, 2021; Sun et al., 2019; Manca et al., 2016; Romero, 2013; Monroy et al., 2010) have demonstrated the importance of the multiporous nature of compacted bentonites in their hydration and swelling. Therefore, it is advisable to use conceptual models that are based on at least a double-porosity approach, the simplest of multiporosity conceptualizations, as a macroscopic basis for simulation. The works of authors such as Moyne and Murad (2003), Mainka et al. (2014), Qiao et al. (2019) and Schreyer Bennethum et al. (1997) provide a robust conceptual foundation for the development of double-porosity models. The conceptual framework that defines the Barcelona Expansive Model (BExM; Alonso et al., 1999), which has been applied with satisfactory results by various authors (Sánchez et al., 2005, 2016; Guimarães et al., 2013; Navarro et al., 2017, 2019; for instance), is adopted in this study.

In the BExM, the behaviour of soil is simulated assuming the coexistence of two superimposed continuous media that interact but are different. According to the original proposal of Gens and Alonso (1992), the microstructural modelling level (m-ML) allows simulation at the macroscopic scale of the effect of the processes that occur inside clay particle aggregates. It is assumed that the existing voids in this space are fundamentally occupied by immobile water (in the sense of Van Genuchten and Wierenga, 1976) linked to the soil skeleton. The macrostructural modelling level (M-ML) introduces the effect of processes that occur in the rest of the pore structure. If an additive formulation is adopted, the rearrangement of the system (characterized by the total strain increase vector, $d\boldsymbol{\varepsilon}$, where, as throughout the paper, Voigt's form is adopted) is modelled by the superposition (sum) of the ordering change induced by the restructuring of the microstructure (strain increment vector $d\boldsymbol{\varepsilon}_{\mathrm{m}}$) and the strains caused by the change in the arrangement of the M-ML voids ($d\boldsymbol{\varepsilon}_{\mathrm{M}}$). To determine $d\boldsymbol{\varepsilon}_{\mathrm{m}}$, models are selected that are elastic, incremental (Sánchez et al., 2005) or based on the

* Corresponding author.
E-mail address: vicente.navarro@uclm.es (V. Navarro).

https://doi.org/10.1016/j.enggeo.2022.106725
Received 17 December 2021; Received in revised form 9 May 2022; Accepted 18 May 2022
Available online 24 May 2022

characterization of the microstructural void ratio e_m (= volume of voids associated with m-ML per volume of solids) through a state surface (Fig. 1; Navarro et al., 2021a). $d\varepsilon_M$ can be defined using the Barcelona Basic Model (BBM; Alonso et al., 1990). In addition, as noted, the interaction $d\varepsilon_{Mm}$ between m-ML and M-ML will be added to $d\varepsilon_M$ and $d\varepsilon_m$.

In hydration processes, depending on the level of confinement, there are two different interaction situations. Under confined conditions, if the soil is packed (overconsolidated soil), the swelling tendency of the aggregates causes the system to restructure, producing a plastic strain $d\varepsilon^{p}_{M\text{-}m}$; this magnitude has been satisfactorily modelled from $d\varepsilon_m$ using the interaction functions proposed by Alonso et al. (1999), developed, among others, by Sánchez et al. (2005). On the other hand, free swelling, $d\varepsilon^{FS}_{M\text{-}m}$, is produced when bentonite is hydrated under low confinement (or unconfined) conditions. Regardless of the level of confinement, hydration is initially mainly located inside the aggregates, i.e., the m-ML pore space. However, if confinement is reduced, as the water content increases, the swelling involves different levels of organization (Saiyouri et al., 2004). That is, the M-ML pore space also increases. As indicated by Cases et al. (1992), when studying sodium montmorillonite, for a high water content (relative humidity greater than 72%), the free swelling "is mainly due to the strong entropic effects linked to the change in the structural organization of the soil, leading to the formation of gel". Saiyouri et al. (2004) also provided an interesting description of the process, noting that swelling is more a subdivision of quasi-crystals than a homogeneous increase in interlayer distances. Salles et al. (2009) and Laird (2006) proposed similar ideas. In the experimental results obtained by Wang et al. (2014) and Cui (2017), a new medium-pore family appeared when swelling was allowed during hydration.

Despite all this valuable information, there is no macroscopic simulation tool that allows describing $d\varepsilon^{FS}_{M\text{-}m}$ for very high values of swelling (void ratios even higher than 20) comparable to those used to describe $d\varepsilon^{p}_{M\text{-}m}$, $d\varepsilon_M$ and $d\varepsilon_m$. Recently, Navarro et al. (2021b) proposed a formulation that allows the simulation of swelling tests performed under different salinity conditions. However, the proposed formulation is markedly heuristic, which compromises its scope. This article proposes a new model with a more solid thermodynamic foundation and, therefore, a more consistent functional structure.

Next, after synthesizing the experimental information used, the conceptual bases and assumed hypotheses are described. Subsequently, the foundation of the constitutive formulation is proposed, and several free swelling tests are simulated to illustrate the scope of the proposed model.

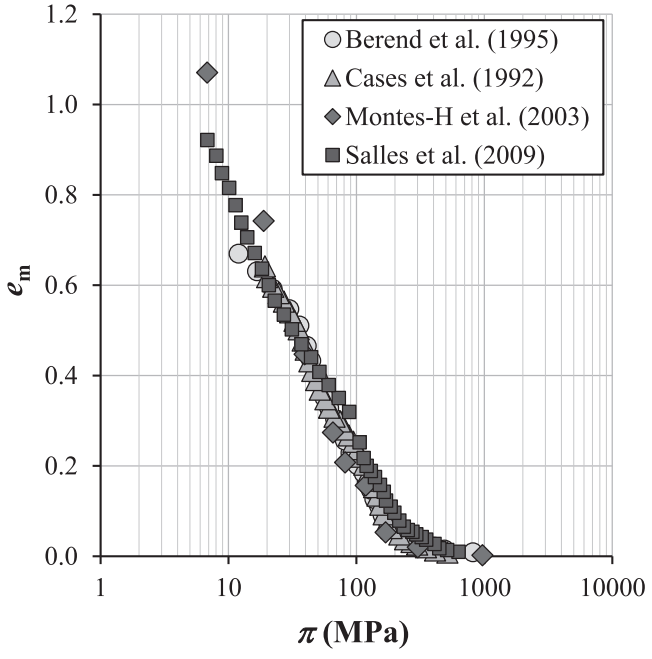

Fig. 1. Variation in the microstructural void ratio e_m with the microstructural effective stress π. Adapted from Navarro et al. (2021a).

2. Material and methods

2.1. Experimental data used

The first set of experimental swelling data used is that measured by Studds et al. (1998) when saturating a Wyoming bentonite powder with chloride salt solutions of different ionic strengths (Fig. 2). The material was mainly formed of Na-montmorillonite, with a liquid limit of 354, a plastic limit of 27, a cation exchange capacity (*CEC*) of 95 mEq/100 g, and a specific gravity equal to 2.751. More data on the material can be found in Studds et al. (1998). In the tests, different chloride solutions with ionic strengths of 0.01, 0.1 or 1 M were used, and practically the same results were obtained for each ionic strength regardless of the chloride solution used.

Subsequently, the results obtained by Dvinskikh and Furó (2009) when saturating cylindrical pellets with a diameter D of 8 mm and height H of 3 mm under conditions of radial confinement and free vertical displacement were analysed. The material used was an MX-80 bentonite that, according to Dvinskikh et al. (2009), was similar to the WyR1 bentonite used by Karnland et al. (2006), so the material parameters estimated by Navarro et al. (2021b) could be used for the material. The pellets initially had a bulk density of 1.8 Mg/m^3 and a water content of 23%. In Figs. 3 and 4, among the different tests performed by Dvinskikh and Furó (2009) with the natural MX-80 bentonite, the most relevant one for the model has been simulated, that is, that in which the material was saturated with deionized (DI) water and presented the greatest swelling and, consistently, higher void ratios. As indicated by Dvinskikh et al. (2009) in the magnetic resonance image investigation of soils, the measured porosity is associated with mobile water, so it was identified in terms of the porosity of the M-ML, e_M (=

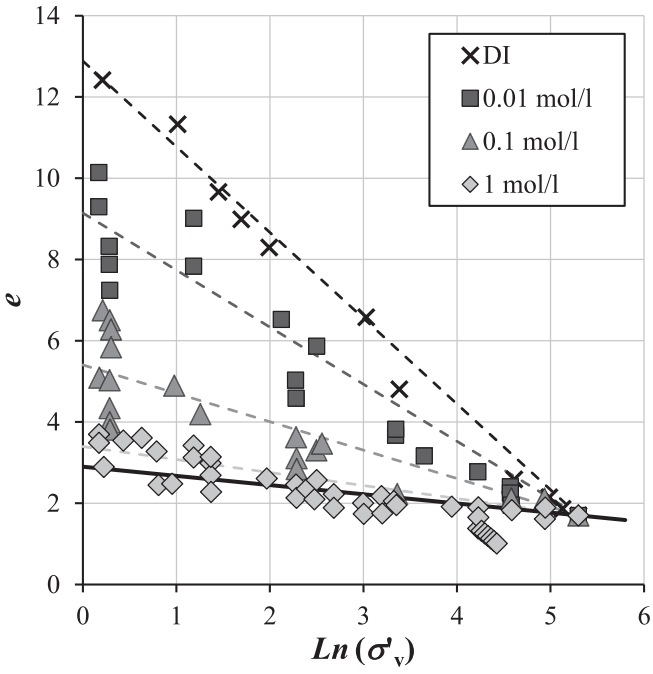

Fig. 2. Swelling of Wyoming bentonite powder when saturated with chloride salt solutions of different ionic strengths. Adapted from Studds et al. (1998). Symbols, experimental results. Dashed lines, ideal response associated with each salinity. Continuous line, estimation of the void ratio variation without free swelling.

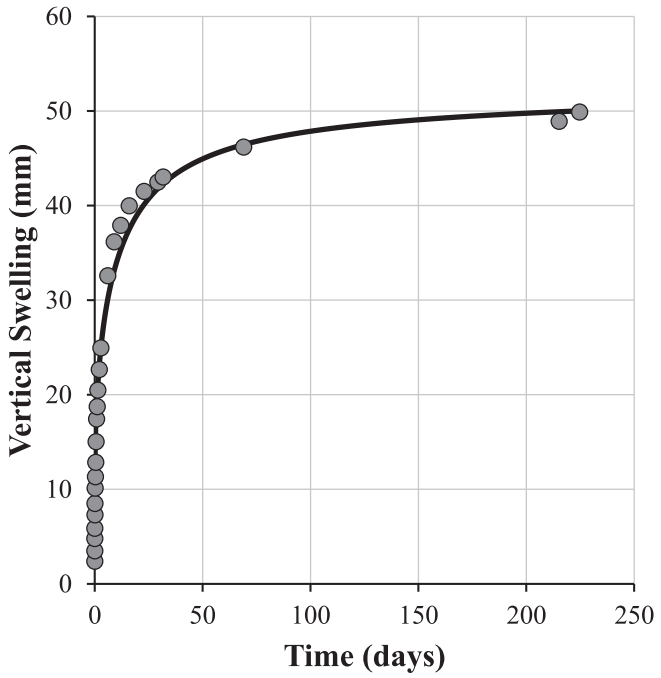

Fig. 3. Comparison between experimental (symbols) and numerical (solid line) swelling in the test by Dvinskikh and Furó (2009).

void volume associated with the M-ML per volume of solids). Both Dvinskikh et al. (2009) and Dvinskikh and Furó (2009) can be consulted for more details of the tests performed.

To analyse the ability of the model to simulate the effect of salinity, the experimental results of the swelling tests described by Navarro et al. (2017) were considered (Fig. 5). In these tests, cylindrical specimens of MX-80 bentonite (similar to the WyR1 of Karnland et al., 2006; again, the parameters estimated for this material have been used) with a D of 50 mm and H of 40 mm were saturated under conditions of radial confinement and free vertical displacement with solutions of different salinities. In addition to a reference test with DI water, solutions of 10 g/L (6.47 g/L NaCl +3.53 g/L CaCl2) and 35 g/L (16.75 g/L NaCl +18.25 g/L CaCl2) were applied. According to Hellä et al. (2014), the first solution simulates the salinity of brackish-saline water that is usually found in Olkiluoto (location of the deep geological repository of spent nuclear fuel in Finland), while the 35 g/L solution simulates the maximum expected salinity. In all cases, the initial bulk density was 2.05 Mg/m^3 with a water content of 17%. More details on the experiments can be found in Navarro et al. (2017).

2.2. Conceptual bases of the model

As indicated in the introduction, free swelling is understood as a large increase in porosity that is experienced by bentonite with low or zero confinement in conditions close to saturation. Before free swelling develops, the increase in the water content of bentonite is essentially associated with the hydration of clay particle aggregates, modelled by the strain $d\varepsilon_m$ of the m-ML. As hydration advances and free swelling begins, the subdivision of particles and aggregates occurs, generating pore space in the M-ML. Although the water that occupies this space ("macrostructural swelling water", MSW) is not immobile, flows in response to hydrodynamic gradients, it has been assumed that it causes a variation in the energy per unit of matter in the system similar to that due to the immobile water of the m-ML. Therefore, a macroscopic approach is adopted in which free swelling is defined by part of the water of the M-ML, the MSW, having the chemical potential μ_m of the m-ML. Consistent with Karnland et al. (2005) and Low and Anderson (1958), μ_m can be calculated as

$$\mu_m = \mu_{VO} + \frac{WMM}{\rho_w}(p - \pi) + \Delta\mu_{mNCC} \quad (1)$$

where μ_{VO} is the chemical potential of free pure water (energy per unit of substance, J/mol SI units), WMM (mass per unit of substance, kg/mol SI units) and ρ_W (mass per unit of volume, kg/m^3) are, respectively, the molecular mass and density of water, p is the net mean stress (Pa ≡ J/m^3), $\Delta\mu_{mNCC}$ (J/mol) is the increase in chemical potential due to the ions (cations and anions) in the microstructure in excess of the CEC (that is, the effect of extra salinity or non-charge-compensating ions on the chemical potential of the microstructural water), and π is the thermodynamic swelling pressure (confinement pressure for a clay in equilibrium, $\mu_m = \mu_{VO}$, with free pure water, $\Delta\mu_{mNCC} = 0$, so that e_m does not

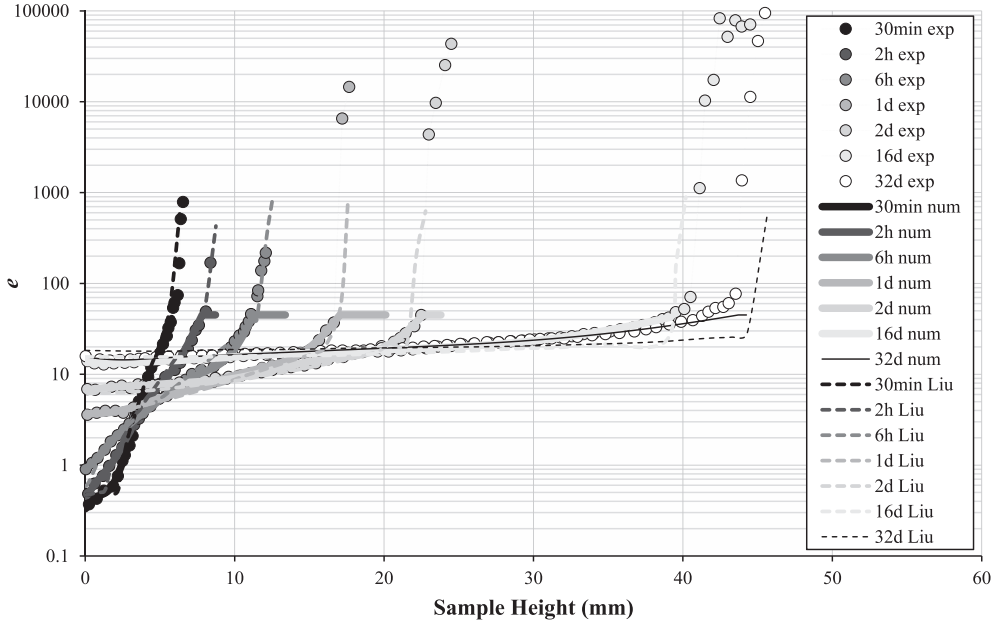

Fig. 4. Comparison of the spatial distribution of the experimental (symbols) and numerical e_M macrostructural void ratio. Solid thick lines, "num", results obtained with the model proposed in this work. Thin solid lines, "Liu", results from Liu et al. (2011) at different times for the Dvinskikh and Furó (2009) test.

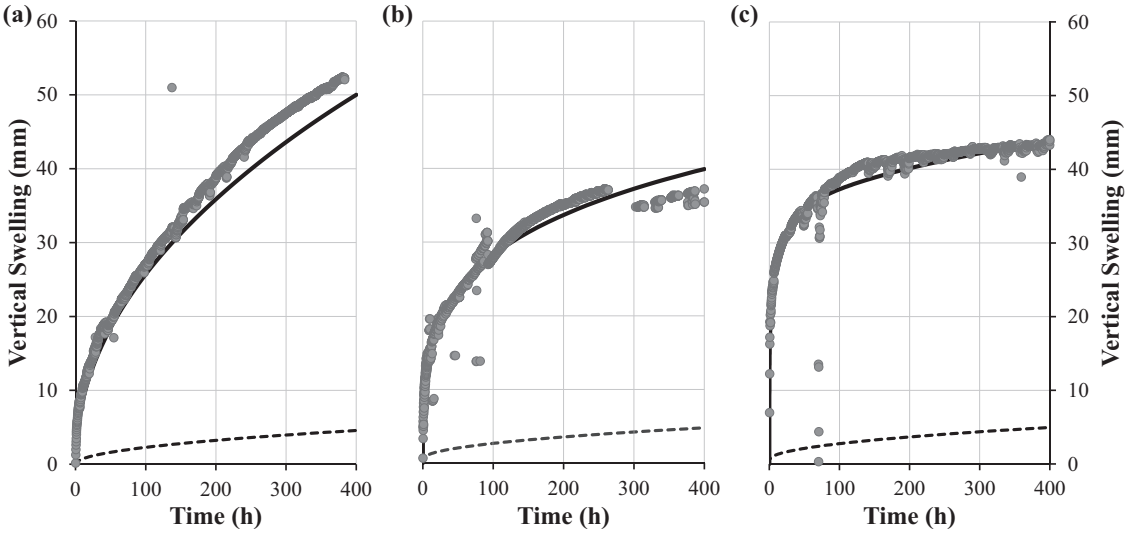

Fig. 5. Comparison of experimental (symbols) and numerical vertical swelling (lines) in the tests of Navarro et al. (2017). Symbols, experimental results. The dashed lines correspond to numerical results obtained without considering the macrostructural swelling ($e_{M\text{-}m} = 0$). (a) DI water, (b) 10 g/L, (c) 35 g/L.

change; Pa ≡ J/m^3), defined by Navarro et al. (2018) according to the microstructural effective stress of bentonite. The chemical potential of the rest of the water in the M-ML is characterized by the chemical potential of the free water μ_M (Edlefsen and Anderson, 1943).

$$\mu_M = \mu_{VO} - \frac{WMM}{\rho_w}(s_M + s_{MO}) \tag{2}$$

where s_M is the macrostructural suction (defined as the capillary suction, $s_M = P_G$ - P_L, where P_G and P_L are the gas and liquid pressures, respectively) and s_{MO} is the osmotic suction of water in the macrostructural aqueous solution.

Consequently, under isothermal conditions, the dissipation dD (defined as indicated in Houlsby and Puzrin, 2000) associated with free swelling can be calculated by adapting the version of the Clausius-Duhem equation proposed by Coussy (2007).

$$dD = \boldsymbol{\sigma}\cdot d\boldsymbol{\varepsilon} + (\mu_m - \mu_M)\, dn - dF \geq 0 \tag{3}$$

where dF is the free energy of the system, $\boldsymbol{\sigma}$ is the total stress vector, and dn is the increase in molar content of swelling water. Under saturated conditions, the increase in M-ML porespace will be equal to the increase in MSW, dn. Therefore, when analysing free swelling processes close to full saturation, this equality will be assumed as a working hypothesis. Then, if a Lagrangian description is adopted in which the energies are expressed with respect to the volume of the solid skeleton, and a fundamentally volumetric swelling process is assumed (an issue to be analysed in future works, as it implies ignoring that the direction of swelling may be conditioned by the orientation of the stress tensor), so that the contribution in the strain work of the deviatoric component of $d\varepsilon^{FS}_{M\text{-}m}$ is assumed to be negligible (it is null under isotropic conditions or in uniaxial conditions),

$$\boldsymbol{\sigma}\cdot d\boldsymbol{\varepsilon} + (\mu_m - \mu_M)\, dn = -(p + \rho_W\cdot(\mu_M - \mu_m))\, de_{M\text{-}m} \tag{4}$$

where p is the mean effective stress, μ_m and μ_M are expressed as energy per unit mass, and $de_{M\text{-}m}$ is the variation in void ratio associated with dn (increase in MSW). That is, $de_{M\text{-}m} = -\, d\varepsilon^{FS}_{M\text{-}m,V}\,(1 + e_O)$, where e_O is the initial value of the total void ratio e (total volume of voids per volume of solid skeleton) and $d\varepsilon^{FS}_{M\text{-}m,V}$ is the volumetric component of $d\varepsilon^{FS}_{M\text{-}m}$. As proposed by Cases et al. (1992), it is assumed that free swelling is an isoenthalpic process. Consequently, at constant temperature T, the dissipation will be equal to $T{\cdot}dS$, where dS is the entropy variation. Therefore, Eqs. (3) and (4) will allow defining the variation of the internal energy of the system per unit volume of solid skeleton, dU, as

$$dU = -(p + \rho_W\cdot(\mu_M - \mu_m))\, de_{M\text{-}m} \tag{5}$$

Assuming saturated conditions, Eq. (4) should be formulated in terms of the effective stresses (Houlsby and Puzrin, 2000). Hence, according to Eqs. (1) and (2), it can be written as

$$dU = -(\pi - \pi_{BS})\, de_{M\text{-}m} \tag{6}$$

where $\pi_{BS} = s_{MO} - \Delta s_{mNCC}$, where Δs_{mNCC} is the expression of $\Delta\mu_{mNCC}$ in units of energy per unit volume ($\Delta s_{mNCC} = \rho_W{\cdot}\Delta\mu_{mNCC}$ / WMM).

The function π_{BS} represents the "saline boundary pressure" (Navarro et al., 2021b). When the water in the M-ML and the m-ML is at equilibrium, $\mu_m = \mu_M$, and, consequently (Eqs. (1) and (2)), $\pi = \pi_B = \pi_{BHM} + \pi_{BS}$, where $\pi_{BHM} = p + s_M$ (where "HM" indicates "hydromechanical"). If the equality between chemical potentials is violated, a mass exchange between the macro- and microstructure will occur. Navarro et al. (2018) introduced π_B to describe this exchange through a mechanical analogy. If, for example, the chemical potential of micro water is lower than that of macro water, π (the pressure "exerted" by the microstructure) will be greater than π_B (the pressure exerted by the macrostructural boundary, "B", on the microstructure), and water will move from the M-ML to the m-ML, increasing e_m. Otherwise, water passes from the m-ML to the M-ML, and e_m decreases.

In the free swelling processes analysed here, in addition to this mass exchange, a difference between μ_m and μ_M will lead to an increase in MSW, $de_{M\text{-}m}$. According to Eq. (6), the scope of this process is fundamentally controlled by π_{BHM}, the value towards $\pi - \pi_{BS}$ tends. Eq. (6) also shows that, in accordance with the experimental observations of authors such as Alawaji (1999) and Navarro et al. (2017), the higher the salinity is, the faster the swelling. In fact, for the same reduction of internal energy, the lower $\pi - \pi_{BS}$ is, the greater its inverse will be, and, consequently, the greater $de_{M\text{-}m}$ will be.

This characteristic of macrostructural swelling should not be confused with another important effect of salinity: the increase in swelling obtained by reducing salinity. Although, as will be seen in the following section, this behaviour is also associated with the increase in MSW, it is largely controlled by the effect that salinity has on the variation in e_m. If salinity decreases, s_{MO} and π_B will be lower (μ_M will be larger). At equilibrium, π becomes larger than π_B (μ_m is smaller than μ_M), and e_m grows as can be seen in Fig. 1. This phenomenon is only "microstructural swelling". Modelling such swelling does not require $d\varepsilon^{FS}_{M\text{-}m}$ to be defined since it is obtained directly from $d\varepsilon_m$.

3. Results and discussion: development and scope of the model

3.1. Constitutive model

In Fig. 2, the responses associated with each salinity obtained by Studds et al. (1998) are approximated by the dashed lines, while the variation in void ratio that would occur without macrostructural swelling is characterized by the continuous line. Therefore, the distance between the two lines defines the free swelling associated with each salinity for each confinement. As noted in Section 2.1, for each ionic strength *IS*, practically the same results were obtained regardless of the kind of chloride solution used. Therefore, to simplify the analysis, in this study, it is assumed that the results correspond to a sodium chloride solution; the ionic strength is calculated from the molal concentration of chloride and sodium ions in the macrostructure, so s_{MO} can be calculated as (Garrels and Christ, 1965)

$$s_{MO} = -\frac{\rho_w}{WMM} R\ T\ Ln(1-0.034\ IS\ ) \tag{7}$$

where R is the universal gas constant. Similarly, Δs_{mNCC} can be estimated as (Navarro et al., 2021b)

$$\Delta s_{mNCC} = -\frac{\rho_w}{WMM} R\ T\ Ln\left(1-0.017\ \left[c_{Cl,m}+c_{Na,m\text{-}NCC}\right]\right) \tag{8}$$

where $c_{Cl,m}$ is the molality of chloride in the microstructure and $c_{Na,m\text{-}NCC}$ is the microstructural non-charge-compensating molal concentration of sodium. Assuming electroneutrality for the two modelling levels, both concentrations can be obtained from the macrostructure values using the Donnan equilibrium approach (Navarro et al., 2021b). For this calculation, it is necessary to determine the microstructural electric charge q

$$q = \frac{CEC\cdot\rho_{mineral}}{e_m} \tag{9}$$

where, as noted in Section 2.1, *CEC* is the cation exchange capacity and $\rho_{mineral}$ is the mineral density, equal to 95 mEq/100 g and 2751 kg/m^3, respectively (Studds et al., 1998). Consequently, for each point in Fig. 2, at equilibrium, e_m (a function of π) will be given byπ_{BHM} (equal to the effective stress in the saturated conditions of the test) andπ_{BS}, which is in turn a function of Δs_{mNCC}. If the nonlinear equation defined by this implicit dependence is solved, then the values of e_m, $e_{M\text{-}m}$, π_{BS} and π can be obtained for each salinity and effective stress when estimating the free swelling as indicated at the beginning of this section. This calculation was achieved by using Eq. (6) to determine the reduction in internal energy dU caused by macrostructural free swelling. Fig. 6 a shows the relative value of U as a function of the variation in the microstructural effective stress, $\Delta\pi$. In all cases, a very good linear correlation is obtained, fulfilling

$$dU = \kappa_{FSW}\, d\pi \tag{10}$$

Therefore, taking into account Eq. (6), we deduce the relationship

$$de_{M\text{-}m} = -\frac{\kappa_{FSW}}{(\pi-\pi_{BS})}d\pi \tag{11}$$

for the constitutive model adopted in this work. In the equation, the slope κ_{FSW}, a log-linear function of salinity (Fig. 6 b), defines the speed with which U is reduced when π also decreases.

3.2. Numerical model

Once $de_{M\text{-}m}$ is defined, $d\varepsilon^{FS}_{M\text{-}m,V}$ can be obtained:

$$d\varepsilon^{FS}{}_{M\text{-}m,V} = -\frac{de_{M\text{-}m}}{(1+e_O)} \tag{12}$$

Furthermore, assuming some spatial distribution of this volumetric magnitude (the simplest is the isotropic condition), $d\varepsilon^{FS}_{M\text{-}m}$ can be calculated. This strain must be considered in the same way that $d\varepsilon^{p}_{M\text{-}m}$, $d\varepsilon_m$, $d\varepsilon^{S}_{M}$ (strain induced by suction changes in the M-ML), $d\varepsilon^{P}_{M}$ (plastic strain caused by the M-ML; generally defined as the strain produced in contact with the load-collapse surface in the BBM; Alonso et al., 1990) or $d\varepsilon^{\sigma}_{M}$ (elastic strain induced by stress changes in the M-ML) when modelling the mechanical behaviour of the system. If a displacement-based finite element formulation is used, the first five strains will be subtracted from the total strain of the system $d\boldsymbol{\varepsilon}$ (obtained through the gradient of the displacement field, $\mathbf{u}$, a state variable of the problem) to obtain $d\boldsymbol{\varepsilon}^{\sigma}_{M}$

$$d\boldsymbol{\varepsilon}^{\sigma}{}_{M} = d\boldsymbol{\varepsilon} - \left(d\boldsymbol{\varepsilon}^{p}{}_{M} + d\boldsymbol{\varepsilon}^{S}{}_{M} + d\boldsymbol{\varepsilon}_m + d\boldsymbol{\varepsilon}^{p}{}_{M\text{-}m} + d\boldsymbol{\varepsilon}^{FS}{}_{M\text{-}m}\right) \tag{13}$$

With this strain and the elastic matrix $\mathbf{D}_M$ of the M-ML, the increase in the constitutive stresses $d\boldsymbol{\sigma}$ can be calculated

$$d\boldsymbol{\sigma} = \mathbf{D}_M\cdot d\boldsymbol{\varepsilon}^{\sigma}{}_{M} \tag{14}$$

For each calculation, the principle of virtual work is applied to solve the mechanical problem (calculation of $\mathbf{u}$). The mass balance equations

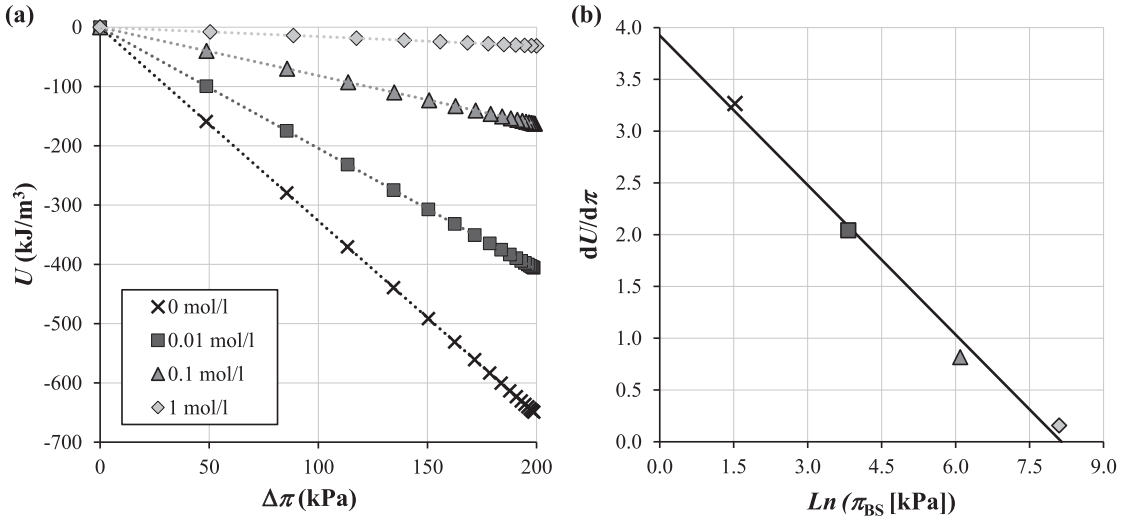

Fig. 6. (a) Variation in internal energy U with decreasing microstructural effective stress π from the research of Studds et al. (1998), Fig. 2. (b) Variation in the slopes of the previous lines as a function of salinity expressed as π_{BS}.

to obtain P_L, P_G and the concentrations of the different chemical species considered (state variables in addition to **u**) are also defined for the resolution of the coupled flow and transport problem. Many of the currently existing numerical models (see, for example, Sánchez et al., 2005, 2016; Guimarães et al., 2013; Navarro et al., 2017, 2019) are based on this calculation strategy. Therefore, the necessary information is available to calculate all the magnitudes involved in Eqs. (1) and (2) (see, for example, Navarro et al., 2021b). Consequently, once a mathematical model of κ_{FSW} has been selected (in this work, we have adopted the model defined in Fig. 6b), it is sufficient to implement Eqs. (11) and (12) to calculate $d\varepsilon^{FS}_{M\text{-}m}$ by modifying the calculation of $d\varepsilon^{\sigma}_{M}$ according to Eq. (13) to adapt existing programs to simulate free swelling processes through the macroscopic formulation proposed here.

3.3. Model scope. Simulation of processes with a large increase in void ratio

As indicated in the previous section, Eq. (11) was introduced into the calculation program developed by Navarro et al. (2019) using the formulation and material parameters of Navarro et al. (2021b). To analyse the scope of this new numerical model, the test of Dvinskikh and Furó (2009) described in Section 2.1 was simulated. As in Dvinskikh et al. (2009), magnetic resonance imaging allowed the quantitative spatial description of the variations in clay density and water content in bentonitic pellets at void ratios up to and greater than 50. To the best of the authors' knowledge, this test is one of the few tests involving the measurement of high expansion values throughout the test time, not only post-mortem. Therefore, this test is a very demanding simulation exercise for the model. However, it is important to note that the proposed formulation is not intended to simulate the extreme values of void ratio obtained in the test, assuming a maximum value of 50. When $e = 50$, Eq. (11) does not apply, assuming $de_{M\text{-}m} = 0$.

Fig. 7 outlines the boundary conditions adopted to simulate the test. The initial conditions were consistent with the initial water content and dry density. The vertical free swelling represented in Fig. 3 was thus obtained. Despite the great expansion observed, the fit to the experimental data is highly satisfactory, especially when taking into account the use of material parameters that were not directly estimated.

The adjustment of the macrostructural void ratio is represented in Fig. 4. The adjustment was performed as in Navarro et al. (2021b), but without performing any parameter estimation to improve the simulation. The fit for pore indices lower than 50 is comparable a to that obtained by Liu et al. (2011) when simulating the test with a model specifically targeting free swelling but that lacks the capacity for macroscopic simulation at an engineering scale and that does not take into account the behaviour of compacted bentonite in confined or partial-saturation conditions. When implemented in a macroscopic model for solving boundary problems at an engineering scale, the proposed formulation can remarkably reproduce not only the trend of the clay volume fraction distribution, but also fits the values over time.

It is interesting to note that the structure of Eq. (11) can reproduce the location of the swelling zone on top of the system where the confinement is lower (in the analysed problem, the effective tension at the top is null) and the increase in void ratio is greater and faster. While Eq. (11) is applied throughout the entire system, it plays the most relevant role at the free edges, where macroscopic swelling is most important.

3.4. Model scope. Analysis of salinity effects on swelling

The results shown in the previous section demonstrate the ability of the model to simulate processes with high expansion. However, for the model to be of practical interest, it must also be able to simulate the effect of salinity on bentonite swelling. To determine whether this is the case, the vertical free swelling tests of Navarro et al. (2017) described in Section 2 were simulated. In the new simulations, the boundary conditions outlined in Fig. 7 were taken, with initial conditions consistent with the initial dry density and water content; the results obtained are presented in Fig. 5. The figure shows that greater swelling is obtained with a lower-salinity soil saturation solution. As indicated in Section 2, the ability to reproduce this behaviour is not only a merit of the $e_{M\text{-}m}$ model but also a consequence of the e_m model. However, macrostructural swelling plays a more important role than microstructural swelling in the production of these differences. If there were no increase in MSW, the relation $e_{M\text{-}m} = 0$ would hold, and the increase in e in the entire domain, but especially in the external boundary, would be considerably lower. The variation in void ratio is represented in Fig. 8b, d and f would occur (for comparison, the initial sample height is used as a reference), so the microstructural swelling would be similar to that indicated by the dashed lines in Fig. 5, much lower than the experimental values. Eq. (11) can reproduce the real behaviour of bentonite and estimate the variations in pore indices represented in Fig. 8a, c and e and the swelling model represented by a continuous line in Fig. 5. Notably, Eq. (11) correctly introduces the reduction in swelling with salinity into the model. Perhaps more importantly, it can also simulate the increase in the swelling rate (Fig. 5) because it reproduces the rapid expansion that

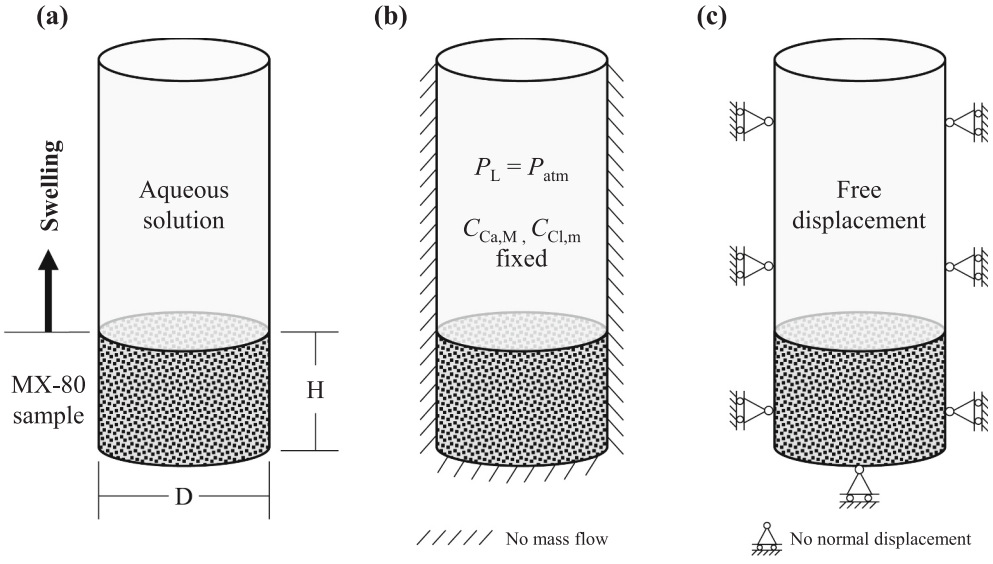

Fig. 7. Boundary conditions adopted when simulating the test of Dvinskikh and Furó (2009) of Fig. 3.

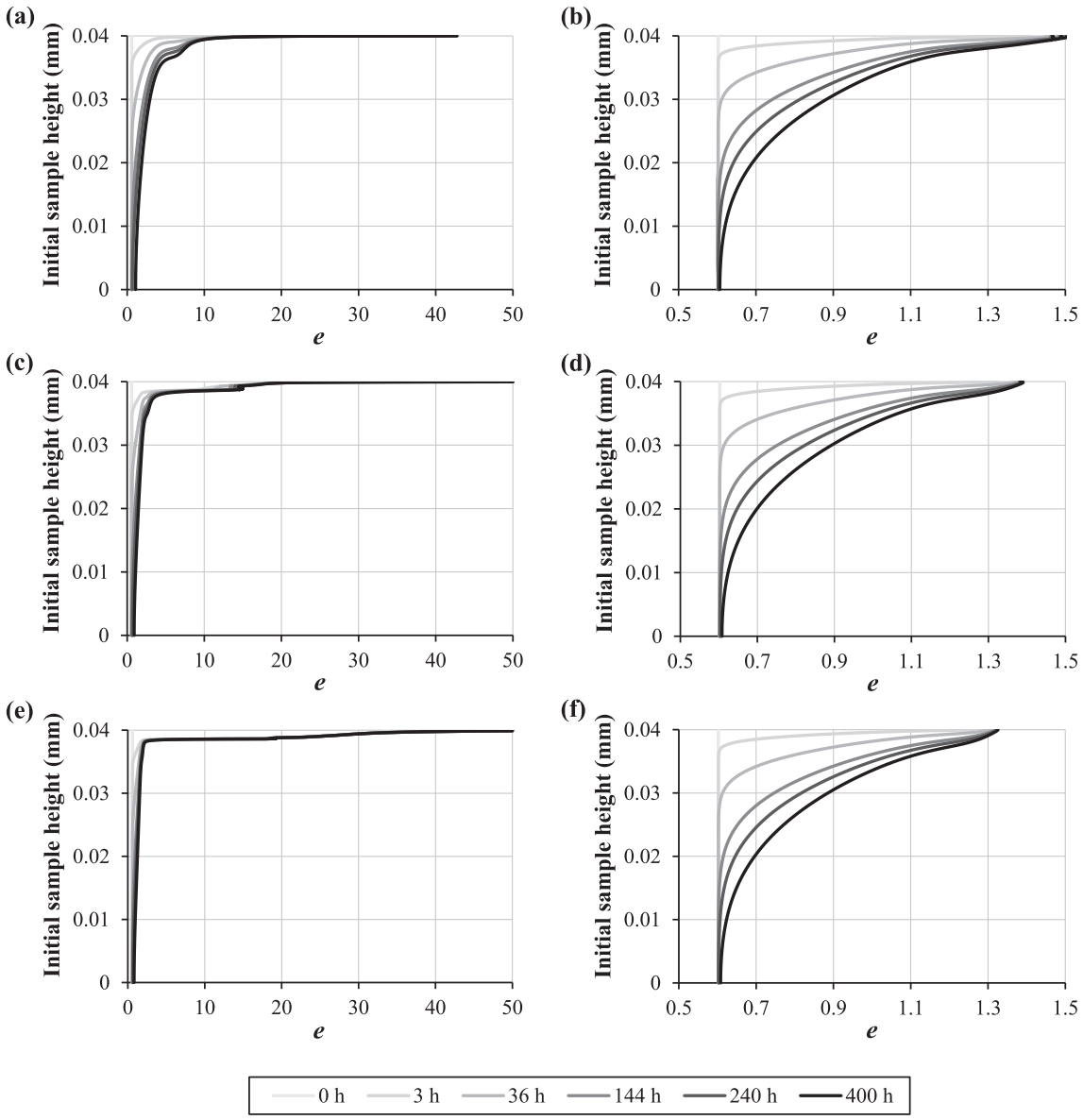

Fig. 8. Distribution of the modelling void ratio in the tests of Navarro et al. (2017) of Fig. 5. Left (Figs. a, c and e), the results using the complete model for DI, 10 g/L and 35 g/L, respectively. Right, the results for the same salinities assuming $de_{M\text{-}m} = 0$. Note the difference in the x-axis scale.

occurs in the external contours when salinity is high. This process is observed in not only Fig. 8a, c and e but also Fig. 9, which shows the variation in the total void ratio at a point initially located 1.2 mm from the top of the sample.

4. Conclusions

A double-porosity macroscopic model has been proposed to simulate the free swelling of bentonites under low confinement conditions. The model is based on the assumption that when hydration increases under these conditions and the subdivision of particles and aggregates occurs, the water that occupies the generated space has a chemical potential that is closer to that of the water of the microstructure than that of the macrostructural bulk water. If isothermal conditions are also assumed, the relevant Clausius-Duhem equation can be used to derive a formal structure to relate the increase in porosity to the decrease in internal energy. Based on this structure and using experimental data from Studds et al. (1998), a constitutive model has been proposed that can determine the increase in void ratio associated with macrostructural swelling as a function of the decrease in microstructural effective stress. According to the implementation strategy described here, the formulation was introduced into a numerical model to solve hydro-chemical-mechanical contour problems at the engineering scale. The developed tool satisfactorily simulated both the total swelling of a specimen and the distribution of the strain when the bentonite reached a void ratio of 50. In addition, both the reduction in swelling with salinity and the increase in swelling rate with increased salinity of the hydration solution were correctly simulated.

CRediT authorship contribution statement

Vicente Navarro: Conceptualization, Data curation, Formal analysis, Funding acquisition, Investigation, Methodology, Project administration, Resources, Software, Supervision, Validation, Visualization, Writing – original draft, Writing – review & editing. **Virginia Cabrera:** Investigation, Resources, Validation, Visualization, Writing – review & editing. **Gema De la Morena:** Investigation, Software, Validation. **Laura Asensio:** Data curation, Funding acquisition, Investigation,

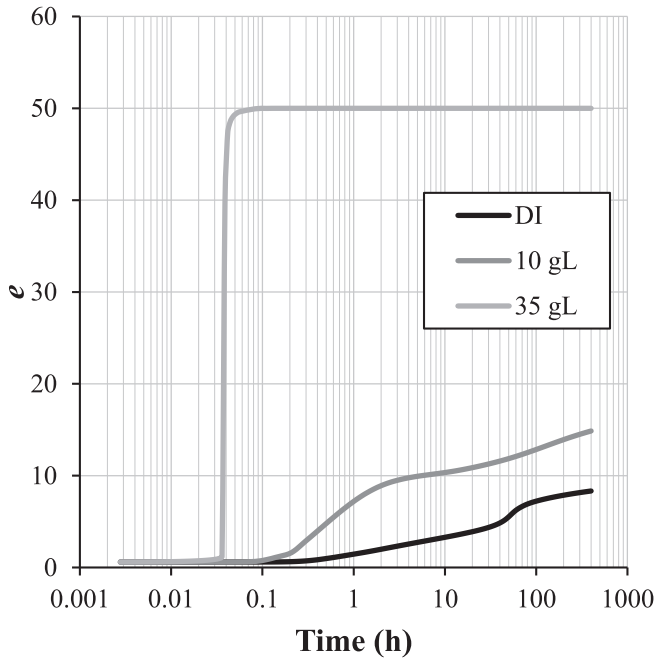

Fig. 9. Estimated variation of the void ratio in the tests of Navarro et al. (2017) at a point initially located 1.2 mm from the top of the sample.

Resources, Software, Writing – review & editing. **Ángel Yustres:** Validation, Visualization, Writing – review & editing. **Joel Torres-Serra:** Formal analysis, Investigation, Validation, Writing – review & editing.

Declaration of Competing Interest

The authors declare that they have no known competing financial interests or personal relationships that could have appeared to influence the work reported in this paper.

Acknowledgements

This study was funded by the Junta de Comunidades de Castilla-La Mancha and the European Regional Development Fund (European Union) through project SBPLY/19/180501/000222.

References

Alawaji, H.A., 1999. Swell and compressibility characteristics of sand-bentonite mixtures inundated with liquids. Appl. Clay Sci. 15 (3–4), 411–430. https://doi.org/10.1016/S0169-1317(99)00033-2.

Alonso, E.E., Gens, A., Josa, A., 1990. A constitutive model for partially saturated soils. Géotechnique. 40 (3), 405–430. https://doi.org/10.1680/geot.1990.40.3.405.

Alonso, E.E., Vaunat, J., Gens, A., 1999. Modelling the mechanical behaviour of expansive clays. Eng. Geol. 54 (1–2), 173–183. https://doi.org/10.1016/S0013-7952(99)00079-4.

Bennett, D.G., Gens, A., 2008. Overview of European concepts for high-level waste and spent fuel disposal with special reference waste container corrosion. J. Nucl. Mater. 379 (1–3), 1–8. https://doi.org/10.1016/j.jnucmat.2008.06.001.

Cases, J.M., Bérend, I., Besson, G., François, M., Uriot, J.P., Thomas, F., Poirier, J.E., 1992. Mechanism of adsorption and desorption of water vapor by homoionic montmorillonite. 1. The sodium-exchanged form. Langmuir 8, 11, 2730–2739. https://doi.org/10.1021/la00047a025.

Coussy, O., 2007. Revisiting the constitutive equations of unsaturated porous solids using a Lagrangian saturation concept. Int. J. Numer. Anal. Methods Geomech. 31 (15), 1675–1694. https://doi.org/10.1002/nag.613.

Cui, Y.J., 2017. On the hydro-mechanical behavior of MX80 bentonite-based materials. J. Rock Mech. Geotech. Eng. 9 (3), 565–574. https://doi.org/10.1016/j.jrmge.2016.09.003.

Delage, P., Tessier, D., 2021. Macroscopic effects of nano and microscopic phenomena in clayey soils and clay rocks. Geomech. Energy Environ. 27, 100177 https://doi.org/10.1016/j.gete.2019.100177.

Dvinskikh, S.V., Furó, I., 2009. Magnetic resonance imaging and nuclear magnetic resonance investigations of bentonite systems. In: SKB Technical Report TR 09–27. Swedish Nuclear Fuel and Waste Management Co., Svensk Kärnbränsleförsörjning AB. https://www.skb.se/publikation/1964192/TR-09-27.pdf (accessed 17 December 2021).

Dvinskikh, S.V., Szutkowski, K., Furó, I., 2009. MRI profiles over very wide concentration ranges: application to swelling of a bentonite clay. J. Magn. Reson. 198 (2), 146–150. https://doi.org/10.1016/j.jmr.2009.01.035.

Edlefsen, N.E., Anderson, A.B.C., 1943. Thermodynamics of soil moisture. Hilgardia. 15 (2), 31–298. https://doi.org/10.3733/hilg.v15n02p031.

Garrels, R.M., Christ, C.H., 1965. Solutions, Minerals, and Equilibria. Harper and Row, New York.

Gens, A., Alonso, E.E., 1992. A framework for the behaviour of unsaturated expansive clays. Can. Geotech. J. 29, 6.

Guimarães, L.D.N., Gens, A., Sánchez, M., Olivella, S., 2013. A chemo-mechanical constitutive model accounting for cation exchange in expansive clays. Géotechnique. 63 (3), 221–234. https://doi.org/10.1680/geot.SIP13.P.012.

Hellä, P., Pitkänen, P., Löfman, J., Partamies, S., Vuorinen, U., Wersin, P., 2014. Safety case for the disposal of spent nuclear fuel at Olkiluoto - definition of reference and bounding groundwaters, buffer and backfill porewaters. In: Posiva Report 2014–04. Posiva Oy. https://inis.iaea.org/collection/NCLCollectionStore/_Public/44/091/44091448.pdf (accessed 17 December 2021).

Houlsby, G.T., Puzrin, A.M., 2000. A thermomechanical framework for constitutive models for rate-independent dissipative materials. Int. J. Plast. 16 (9), 1017–1047. https://doi.org/10.1016/S0749-6419(99)00073-X.

Karnland, O., Muurinen, A., Karlsson, F., 2005. Bentonite swelling pressure in NaCl solutions - experimentally determined data and model calculations. In: Alonso, E.E., Ledesma, A. (Eds.), Advances in Understanding Engineered Clay Barriers: Proceedings of the International Symposium on Large Scale Field Tests in Granite, Sitges, Barcelona, 12–14 November 2003. Taylor and Francis Group, London, pp. 241–256.

Karnland, O., Olsson, S., Nilsson, U., 2006. Mineralogy and sealing properties of various bentonites and smectite-rich clay materials. In: SKB Technical Report TR-06-30. Swedish Nuclear Fuel and Waste Management Co., Svensk Kärnbränslehantering AB. http://www.skb.se/upload/publications/pdf/TR-06-30.pdf (accessed 17 December 2021).

Laird, D.A., 2006. Influence of layer charge on swelling of smectites. Appl. Clay Sci. 34 (1–4), 74–87. https://doi.org/10.1016/j.clay.2006.01.009.

Liu, L., Neretnieks, I., Moreno, L., 2011. Permeability and expansibility of natural bentonite MX-80 in distilled water. Phys. Chem. Earth Parts A/B/C 36 (17–16), 1783–1791. https://doi.org/10.1016/j.pce.2011.07.009.

Low, P.F., Anderson, D.M., 1958. Osmotic pressure equations for determining thermodynamic properties of soil water. Soil Sci. 86 (5), 251–253. https://doi.org/10.1097/00010694-195811000-00004.

Mainka, J., Murad, M., Moyne, C., Sidarta, A.L., 2014. A modified effective stress principle for unsaturated swelling clays derived from microstructure. Vadose Zone J. 13, 5. https://doi.org/10.2136/vzj2013.06.0107.

Manca, D., Ferrari, A., Laloui, L., 2016. Fabric evolution and the related swelling behaviour of a sand/bentonite mixture upon hydro-chemo-mechanical loadings. Géotechnique 66 (1), 41–57. https://doi.org/10.1680/jgeot.15.P.073.

Monroy, R., Zdravkovic, L., Ridley, A., 2010. Evolution of microstructure in compacted London Clay during wetting and loading. Géotechnique 60 (2), 105–119. https://doi.org/10.1680/geot.8.P.125.

Moyne, C., Murad, M., 2003. Macroscopic behavior of swelling porous media derived from micromechanical analysis. Transp. Porous Media 50, 127–151. https://doi.org/10.1023/A:1020665915480.

Navarro, V., Yustres, Á., Asensio, L., De la Morena, G., González-Arteaga, J., Laurila, T., Pintado, X., 2017. Modelling of compacted bentonite swelling accounting for salinity effects. Eng. Geol. 223, 48–58. https://doi.org/10.1016/j.enggeo.2017.04.016.

Navarro, V., De la Morena, G., González-Arteaga, J., Yustres, Á., Asensio, L., 2018. A microstructural effective stress definition for compacted active clays. Geomech. Energy Environ. 15, 47–53. https://doi.org/10.1016/j.gete.2017.11.003.

Navarro, V., Asensio, L., Gharbieh, H., De la Morena, G., Pulkkanen, V.-M., 2019. Development of a Multiphysics numerical solver for modeling the behavior of a clay-based engineered barriers. Nucl. Eng. Technol. 51 (4), 1047–1059. https://doi.org/10.1016/j.net.2019.02.007.

Navarro, V., Yustres, Á., Jenni, A., De la Morena, G., Asensio, L., López-Vizcaíno, R., Cabrera, V., Wersin, P., Mäder, U., Muuri, E., Niskanen, M., Akinwunmi, B., Hirvi, J. T., Pakkanen, T.A., 2021a. Molecular dynamics data for modelling the microstructural behaviour of compacted sodium bentonites. Appl. Clay Sci. 201, 105932 https://doi.org/10.1016/j.clay.2020.105932.

Navarro, V., De la Morena, G., Alonso, J., González-Arteaga, J., Asensio, L., 2021b. Numerical model of free swelling processes in compacted MX-80 bentonites. Int. J. Rock Mech. Min. Sci. 141, 104713 https://doi.org/10.1016/j.ijrmms.2021.104713.

Qiao, Y., Xiao, Y., Laloui, L., Ding, W., He, M., 2019. A double-structure hydromechanical constitutive model for compacted bentonite. Comput. Geotech. 115, 103173 https://doi.org/10.1016/j.compgeo.2019.103173.

Romero, E., 2013. A microstructural insight into compacted clayey soils and their hydraulic properties. Eng. Geol. 165, 3–19. https://doi.org/10.1016/j.enggeo.2013.05.024.

Saiyouri, N., Tessier, D., Hicher, P.Y., 2004. Experimental study of swelling in unsaturated compacted clays. Clay Miner. 39 (4), 469–479. https://doi.org/10.1180/0009855043940148.

Salles, F., Douillard, J.M., Denoyel, R., Bildstein, O., Jullien, M., Beurroies, I., Van Damme, H., 2009. Hydration sequence of swelling clays: evolutions of specific surface area and hydration energy. J. Colloid Interface Sci. 333, 2. https://doi.org/10.1016/j.jcis.2009.02.018.

Sánchez, M., Gens, A., Guimarães, L.D.N., Olivella, S., 2005. A double structure generalized plasticity model for expansive materials. Int. J. Numer. Anal. Methods Geomech. 29 (8), 751–787. https://doi.org/10.1002/nag.434.

Sánchez, M., Gens, A., Villar, M.V., Olivella, S., 2016. Fully coupled thermo-hydro-mechanical double-porosity formulation for unsaturated soils. Int. J. Geomech. 16, 6.

Schreyer Bennethum, L., Murad, M.A., Cushman, J.H., 1997. Modified Darcy's law, Terzaghi's effective stress principle and Fick's law for swelling clay soils. Comput. Geotech. 20 (3–4), 245–266. https://doi.org/10.1016/S0266-352X(97)00005-0.

Sellin, P., Leupin, O.X., 2013. The use of clay as an engineered barrier in radioactive waste management - a review. Clay Clay Miner. 61 (6), 477–498. https://doi.org/10.1346/CCMN.2013.0610601.

Studds, P.G., Stewart, D.I., Cousens, T.W., 1998. The effects of salt solutions on the properties of bentonite-sand mixtures. Clay Miner. 33 (4), 651–660. https://doi.org/10.1180/000985598545804.

Sun, H., Mašín, D., Najser, J., Neděla, V., Navrátilová, E., 2019. Bentonite microstructure and saturation evolution in wetting–drying cycles evaluated using ESEM, MIP and WRC measurements. Géotechnique. 69 (8), 713–726. https://doi.org/10.1680/jgeot.17.P.253.

Van Genuchten, M.T., Wierenga, P.J., 1976. Mass transfer studies in sorbing porous media I. Analytical solutions. Soil Sci. Soc. Am. J. 40, 4, 473–480. https://doi.org/10.2136/sssaj1976.03615995004000040011x.

Wang, Q., Cui, Y.J., Tng, A.M., Li, X.L., Ye, W.M., 2014. Time- and density-dependent microstructure features of compacted bentonite. Soils Found. 54 (4), 657–666. https://doi.org/10.1016/j.sandf.2014.06.021.